Single-cell characterization and metabolic profiling of in vitro cultured human skeletal progenitors with enhanced in vivo bone forming capacity

Johanna Bolander, Tim Herpelinck, Malay Chaklader, Charikleia Gklava, Liesbet Geris, Frank P. Luyten

TISSUE ENGINEERING AND REGENERATIVE MEDICINE

STEM CELLS
TRANSLATIONAL MEDICINE

Single-cell characterization and metabolic profiling of in vitro cultured human skeletal progenitors with enhanced in vivo bone forming capacity

Johanna Bolander[1,2] 🆔 | Tim Herpelinck[1,2] | Malay Chaklader[1,2] | Charikleia Gklava[1,2] | Liesbet Geris[2,3,4] | Frank P. Luyten[1,2]

[1]Tissue Engineering Laboratory, Skeletal Biology and Engineering Research Center, KU Leuven, Leuven, Belgium

[2]Prometheus, Division of Skeletal Tissue Engineering, KU Leuven, Leuven, Belgium

[3]Biomechanics Section, KU Leuven, Leuven, Belgium

[4]Biomechanics Research Unit, GIGA in silico medicine, University of Liege, Liège, Belgium

Correspondence
Frank P. Luyten, MD, PhD, Skeletal Biology and Engineering Research Center, O&N I Herestraat 49 - box 813 13, 3000 Leuven, Belgium.
Email: frank.luyten@uzleuven.be

Funding information
Hercules Foundation; B.A.E.F. Henri Benedictus Fellowship; Research Foundation - Flanders, Grant/Award Numbers: 1S80019N, 12S6817N, 1518618N

Abstract

Cell populations and their interplay provide the basis of a cell-based regenerative construct. Serum-free preconditioning can overcome the less predictable behavior of serum expanded progenitor cells, but the underlying mechanism and how this is reflected in vivo remains unknown. Herein, the cellular and molecular changes associated with a cellular phenotype shift induced by serum-free preconditioning of human periosteum-derived cells were investigated. Following BMP-2 stimulation, preconditioned cells displayed enhanced in vivo bone forming capacity, associated with an adapted cellular metabolism together with an elevated expression of BMPR2. Single-cell RNA sequencing confirmed the activation of pathways and transcriptional regulators involved in bone development and fracture healing, providing support for the augmentation of specified skeletal progenitor cell populations. The reported findings illustrate the importance of appropriate in vitro conditions for the in vivo outcome. In addition, BMPR2 represents a promising biomarker for the enrichment of skeletal progenitor cells for in vivo bone regeneration.

KEYWORDS

bone, cell surface markers, cell signaling, mesenchymal stem cells (MSCs), serum-free, tissue engineering, tissue regeneration, tissue-specific stem cells

1 | INTRODUCTION

Cell-based constructs represent an attractive alternative strategy for restoring the function of damaged organs or tissues where currently no reliable treatment is available today.[1–3] Key in the construct's success lies in a bioinspired design, typically based on appropriate and potent progenitor cells, which upon stimulation and implantation direct tissue repair together with the available host environment to facilitate integration.[4,5] In consequence, the cell source may define the tissue-forming potential of the construct, whereas a carefully developed manufacturing process with appropriately selected culture and priming conditions appears primordial. Nonunion bone fractures are typically caused by a lack of a sufficient number of appropriate progenitor cells to bridge the defect.[6] With this principle in mind for the treatment of large long bone defects, human periosteum-derived cells (hPDCs) represent a clinically relevant source of progenitor cells due to their crucial role in postnatal fracture healing.[7,8] Similarly to in vivo fracture healing in mice,[9] in vitro expanded hPDCs delivered on a ceramic scaffold require active bone morphogenetic protein (BMP)-signaling during ectopic in vivo bone formation.[10] Notably, exogenous BMP-stimulation could further enhance the bone forming capacity.[11] Moreover, it was reported that the osteochondrogenic potential of in

vitro expanded hPDCs could be associated with elevated mRNA transcripts of the BMP type 1 and type 2 receptors.[12] This is of particular interest since BMP-ligands are indispensable stimulatory factors in the periosteum during fracture healing[13] and signal through a complex of type 1 (ALK1/ACVRL1, ALK2/ACVR1, ALK3/BMPR1A, and ALK6/BMPR1B) and type 2 (BMPR2, ACVR2A, and ACVR2B) transmembrane serine/threonine kinase receptors. As such, the expression level and availability of the BMP-receptors on a progenitor cell is crucial for their ability to respond and undergo subsequent differentiation upon BMP-stimulation.[14]

Unfortunately, this part is often a neglected parameter in the preparation and characterization of cell-based constructs. Instead, current progenitor markers are selected based on the cells' ability to proliferate and differentiate under nonphysiological conditions.[15,16] Indeed, the use of platelet lysate or serum may have a proliferative effect, but involves an uncontrolled cocktail of factors introducing issues with repeatability, potency, and control of the process. Instead, serum-free culture systems were recently reported to stabilize the quality and the purity of the cell population.[17] As an outcome, these features can improve reliability, reproducibility, and robustness of the manufacturing process and be more predictive of the in vivo outcome.

In the present study, we elucidate the mechanism of the improved biological potency of serum-free preconditioning of serum-expanded hPDCs, resulting in elevated ectopic and orthotopic bone forming capacity depending on active BMPR2-signaling. Detailed analysis by single-cell RNA sequencing confirmed that preconditioning induced a phenotype switch, potentially reflecting the regenerative activation of the progenitor cells as well as a clear shift in cellular metabolism. Combined, the presented findings provide a detailed and novel characterization protocol of a potent cell-based construct. We believe that these findings will inspire to develop more relevant culture conditions for progenitor cells and function as a guide regarding characterization strategies for regulatory bodies.

2 | MATERIALS AND METHODS

In vitro expanded hPDCs were preconditioned in a serum-free chemically defined medium (CDM) or growth medium (GM) containing 10% FBS as control for 6 days. Directly following preconditioning, stimulation with BMP-2-supplemented CDM or GM was carried out on monolayer cultures for an additional 6 days. *In vivo* evaluation was performed ectopically and orthotopically in NMRI[nu/nu] mice. For this, cells were seeded onto CopiOs (Zimmer, Wemmel, Belgium) CaP-matrices followed by implantation. *In vivo* development of the implanted constructs was studied up to 8 weeks. Detailed materials and methods are provided in Supplemental Information. The ethical committee for Human Medical Research (KU Leuven) approved all procedures, and the patient informed consents were obtained. The animals were housed according to the guidelines of the Animalium Leuven (KU Leuven). Detailed materials and methods are provided in Supplemental Materials and Methods.

Significance statement

A critical number of in vitro expanded progenitor cells provide the key driving force in a cell-based regenerative construct. Standard expansion protocols highly affect the initial cellular phenotype due to the focus on fast expansion rather than on the maintenance of the progenitor potential. This article describes a serum-free preconditioning regime of in vitro expanded human periosteum-derived cells that lead to a progenitor cell with enhanced in vivo bone forming capacity at the single cell level. This phenotype shift was associated with an adapted cellular metabolism and activation of pathways and transcriptional regulators involved in bone development and fracture healing, illustrating the importance of appropriate in vitro conditions for the in vivo outcome.

3 | RESULTS

3.1 | CDM preconditioning causes metabolic adaptation

The metabolism and physiology of progenitor cells are dependent on their cell state and environment. Therefore, we initially investigated the temporal profiles of progenitor and differentiation state in hPDCs in terms of morphology and marker expression upon serum-free preconditioning in a chemically defined medium (CDM) as compared with standard serum-containing growth medium (GM) culture. During a 9-day culture period, CDM was confirmed to maintain viability without cell proliferation while an upregulation of skeletal progenitor markers was observed including Vascular endothelial growth factor receptor (*VEGFR*), Platelet-derived growth factor receptor (*PDGFR*)β/α, Vascular-endothelial (*VE*)-*Cadherin* (Figure S1). Upon supplementing the GM or CDM with BMP-2 in the preconditioned hPDCs, upregulated osteochondrogenic differentiation was seen in the CDM-primed cells, as reflected by a significant upregulation of chondrogenic markers *SOX9*, Collagen type (*COLL*)2 and *COLL10* as well as for the osteogenic markers Runt-related transcription factor (TF) (*RUNX*)2, Osterix (*OSX*), and *COLL1* (Figure S2). The temporal profiles of mRNA transcripts showed that 6 days of preconditioning followed by 6 days of BMP-2 priming induced a significant cellular adaptation and differentiation when compared with serum containing conditions (Figures S1 and S2). In order to evaluate whether the shift in progenitor state was also affected on metabolic level, we investigated the temporal adaptation in metabolite concentrations in conditioned medium. In addition, we evaluated mRNA transcript levels of markers involved in multiple metabolic pathways during preconditioning and BMP-2 priming in CDM compared with GM cultures. Measurements of glucose and lactate in the conditioned medium revealed that hPDCs cultured in GM are highly glycolytic in comparison to CDM cultured cells (Figure 1A,B). At day 6, it was shown that prolonged culture time further elevated the difference in
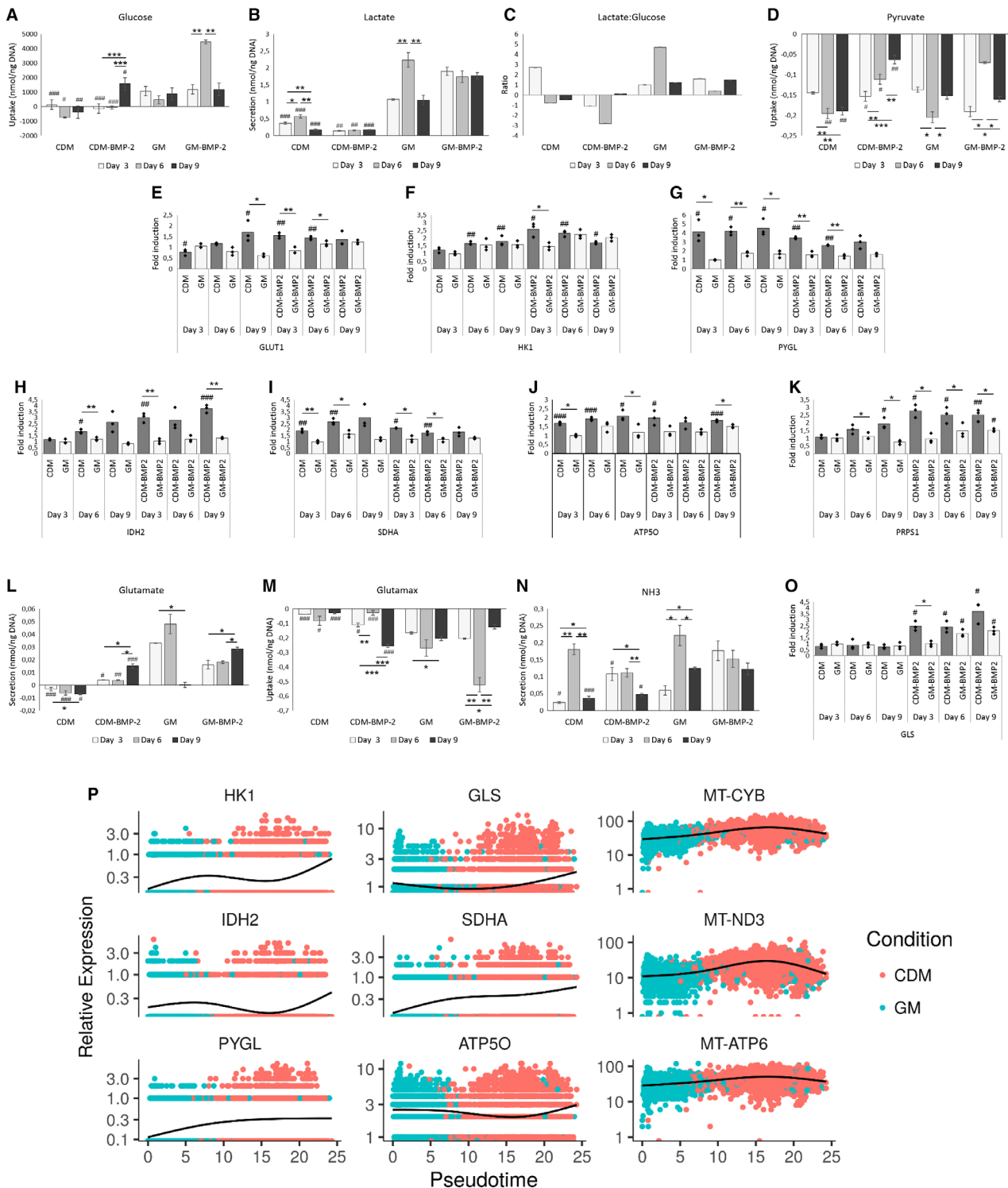
FIGURE 1 Adapted metabolism in chemically defined medium (CDM)-cultured cell populations. Analysis of metabolites in conditioned medium and mRNA transcript analysis of metabolic markers in preconditioned and BMP-2 primed cells in CDM or growth medium (GM). Measurements of glycolytic metabolites in conditioned medium: glucose (A), lactate (B), ratio lactate:glucose (C), and pyruvate (D). mRNA transcript analysis of associated markers *GLUT1* (E), *HK1* (F), *PYGL* (G), *IDH2* (H), *SDHA* (I), *ATP5O* (J), and *PRPS1* (K). Measurements on the conditioned medium for amino acid metabolism: glutamate (L), glutamax (M), NH_3 (N), and mRNA transcript analysis of *GLS1* (O). Trajectory analysis displaying the relative gene expression of *HK1, IDH2, PYGL, GLS1, SDHA, ATP5O*, and the mitochondrial (MT) genes *CYB, ND3, ATP6* vs pseudotime (P). Statistical significance: *P*-value: * < .05, ** < .01, *** < .001 or # < .05, ## < .01, ### < .001 to GM (A, B, D, L, M, N) or day 0 (E-K, O)

glycolytic activity, as indicated by a strong increase in the lactate:glucose ratio (Figure 1C). The glycolytic activity coincided with increased pyruvate uptake (Figure 1D) and was reflected on the gene expression level by increased expression of glucose transporter 1 (*GLUT1*) at day 3 and hexokinase 1 (*HK1*) by day 6 (Figure 1E,F). In addition, the elevation in glycogen phosphorylase liver isoform (*PYGL*) expression levels indicated the potential recruitment of glucose from the glycogen stores to maintain the energy balance in the CDM cultured cells (Figure 1G). Interestingly, the addition of BMP-2 to the medium induced higher glucose consumption in GM cultures but did not affect the overall glucose:lactate ratio,

suggesting that the cells remained strongly glycolytic. This view was further reinforced by the increased expression of *GLUT1* and *HK1*. Of note, the strongly increased uptake of glucose at day 6 of BMP stimulation was accompanied by a decreased uptake of pyruvate.

These results suggested that preconditioning in CDM led to cells becoming less glycolytic, as reflected by the lactate:glucose ratio. In addition, the expression of *PYGL* was strongly enhanced, further indicative of glycogenolysis. Moreover, the increased pyruvate uptake combined with the elevated expression levels of isocitrate dehydrogenase (*IDH2*), succinate dehydrogenase subunit A (*SDHA*), and ATP
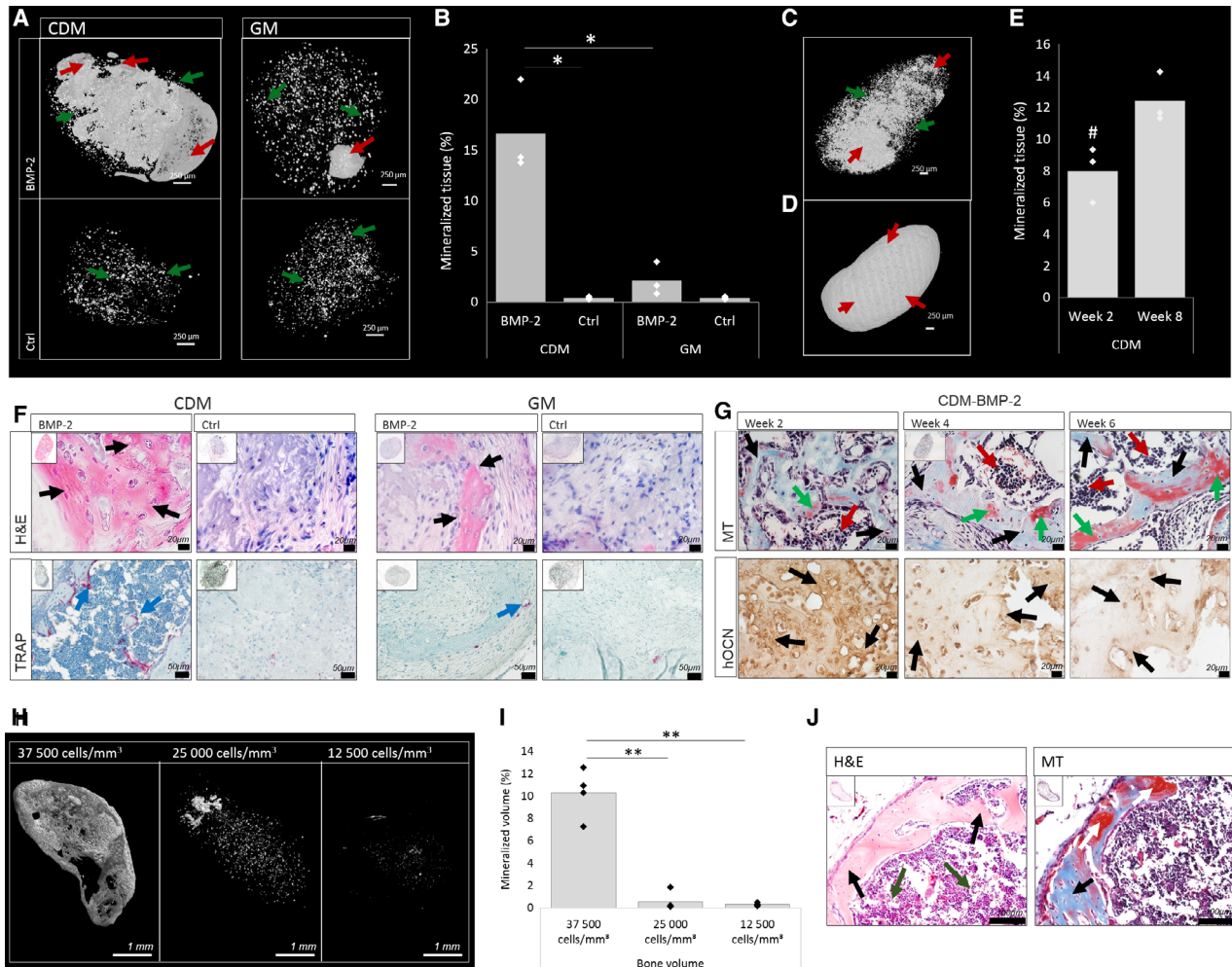

FIGURE 2 Elevated in vivo bone formation by in vitro BMP-2 stimulated human periosteum-derived cells (hPDCs) under serum-free conditions. Upon in vivo implantation of in vitro BMP-2 stimulated hPDCs seeded onto CopiOs scaffolds at 50,000 cells/mm³, constructs scanned by nano-CT for 3D visualization displayed mineralized tissue after 4 weeks of implantation (red arrows), but not in nonstimulated controls where only scaffold remnants were seen (green arrows) (A). Quantification of mineralized tissue normalized to total explant volume (B). The mineralization in constructs containing serum-free stimulated hPDCs had started at 2 weeks (C) whereas a more mineralized and dense tissue was seen in the same condition after 8 weeks (D). Quantification confirmed a higher percent of mineralized tissue at week 8 (E). Qualitative analysis after 4 weeks confirmed bone formation in constructs containing BMP-2-stimulated cells by hematoxylin and eosin (H&E) staining (black arrows) whereas remodeling of the newly formed bone was confirmed by a TRAP staining (blue arrows) (F). In the BMP-2/CDM condition, Masson's trichrome (MT) staining confirmed presence of mature bone regions (green arrows) and bone marrow formation (red arrows). The appearance of early mineralized tissue after 2 weeks in the BMP-2/CDM-condition was confirmed by MT staining (black arrows) while graft contribution was depicted by hOCN (G). nano-CT scans upon 4 weeks implantation of CaP-matrix seeded with 37.5, 25, and 12.5 × 10³ primed hPDCs/mm³ scaffold (H) and quantified mineralized tissue formation (I). H&E and MT confirmed bone (black arrows) and bone marrow (gray arrows) while Alcian blue (AB) staining confirmed GAG rich areas (gray arrows) (J). Statistical significance: *P*-value: * < .05, ** < .01, *** < .001 and #< .05 to week 4. Scale bar: A-D: 250 µm; F-G: 20 µm H&E, MT, and hOCN, 50 µm TRAP; H: 1 mm; J: 100 µm

synthase subunit 5O (*ATP5O*) (Figure 1H-J) suggest a shift toward oxidative phosphorylation as a main source of energy. Unsupervised construction of an inferred pseudotime trajectory using Monocle2[18] on single-cell RNA sequencing data supported the transitional upregulation of *HK1*, *IDH2*, *PYGL*, and *SDHA* together with upregulation of mitochondrial genes *MT-CYB*, *MT-ND3*, and *MT-ATP6* upon transfer from GM cultures to CDM (Figure 1P). This potential adaptation continued upon BMP stimulation, with a decreased dependence on glycogen. Interestingly, BMP-2 induced increased gene expression of phosphoribosyl pyrophosphate synthetase 1 (*PRPS1*) (Figure 1K) indicating increased *de novo* nucleotide biosynthesis and potentially an increased need for reductive potential through the pentose phosphate shunt.

Taken together, these data indicate that hPDCs are highly glycolytic during expansion in GM, which is largely unaffected by BMP stimulation under serum containing conditions. Conversely, preconditioning in CDM appears to abrogate glycolytic activity to induce a shift toward oxidative phosphorylation, potentially accompanied by recruitment of the glycogen stores.

Analysis of the amino acid metabolism demonstrated a high production of glutamate during expansion in GM (Figure 1L). At day 6 of expansion, cells in GM displayed increased glutamine uptake and NH_3 production (Figure 1M,N), suggesting that the increased concentrations of glutamate are converted from glutamine. However, BMP stimulation reduced the production of glutamate and NH_3, while increasing glutamine consumption and expression of glutaminase (*GLS1*) (Figure 1O). Consequently, BMP-2 appears to increase the need for reductive potential and stimulates nucleotide synthesis, but does not affect energy homeostasis.

3.2 | Enhanced in vitro differentiation resulted in elevated ectopic in vivo bone formation

To evaluate the enhanced differentiation potential and the altered metabolic profile seen in CDM cultures, BMP-2 primed cells were seeded onto a CaP-matrix with no in vivo bone forming capacity when seeded with nonprimed hPDCs. Subsequently, constructs were implanted in an ectopic NMRI[nu/nu] mouse model for 4 weeks. Analysis of 3D reconstructed nano-CT scans displayed various tissue formation profiles by the different constructs (Figure 2A). Both CDM and GM cultures supplemented with BMP-2 displayed *de novo* formation of mineralized tissue (red arrows, Figure 2A). Of note, the newly formed tissue was both larger and more homogeneous in the CDM condition. In control explants seeded with preconditioned but not BMP-2 stimulated hPDCs, only remnants of CaP-grains from the scaffold were seen (green arrows, Figure 2A). Upon quantification, a 10-fold higher amount of mineralized matrix was observed at 4 weeks in constructs seeded with hPDCs treated with BMP-2 supplemented CDM, as compared to constructs containing cells stimulated under GM conditions (Figure 2B). Due to the clear difference in *de novo* formed bone in CDM-BMP-2 cultures, explants at 2 and 8 weeks were investigated. Mineralized tissue was detected from 2 weeks on (Figure 2C). By

week 8, the bone tissue had fully matured (Figure 2D). Upon quantification, there was an increase in mineralized tissue formation at week 4 and 8, as compared with week 2, in CDM cultures supplemented with BMP-2 (Figure 2E).

Qualitative tissue analysis was carried out by histology and IHC. At 4 weeks, *de novo* bone tissue was found in sections containing BMP-2 stimulated cells, depicted by hematoxylin and eosin (H&E) staining (black arrows, Figure 2F). Active remodeling was suggested by areas positive for TRAP staining in the BMP-2 stimulated constructs (blue arrows). In BMP-2 supplemented CDM conditions, the presence of areas of different maturity was confirmed by a Masson's trichrome (MT) staining, as reflected by intensity in blue (black arrows) for different densities and red stain for mature bone tissue (green arrows, Figure 2G). Moreover, this staining displayed bone marrow infiltration (red arrows) in the zones of early mineralized tissue (Figure 2G). Contribution to *de novo* formed bone by the implanted cells was confirmed by IHC for human osteocalcin (hOCN) (Figure 2G). In order to evaluate whether the CDM preconditioned cells possessed higher bone forming capacity per cell, reduced cell seeding density was evaluated using 37,500, 25,000, and 12,500 $hPDCs/mm^3$ and compared with the initial density of 50,000 $hPDC/mm^3$ scaffold. Robust and homogenous bone formation was seen when 37,500 $hPDCs/mm^3$ was used while limited bone formation was seen with 25,000 $hPDCs/mm^3$ and no bone formation in the 12,500 $hPDC/mm^3$ condition (Figure 2H-J and Figure S3). In summary, these data indicate that the enhanced *in vitro* differentiation capacity as a result of serum-free preconditioning could be correlated to improved bone forming capacity in vivo where implanted cells formed ectopic bone through the endochondral route.

3.3 | Healing of a critical size long-bone defect by serum-free in vitro BMP-2 stimulated hPDCs

Based on the ectopic endochondral bone formation of the serum-free in vitro primed cells, the orthotopic behavior was next assessed in a critical size tibial defect in athymic mice. Upon implantation, the in vivo behavior of the in vitro CDM-BMP-2 primed cells seeded onto a CaP-carrier was analyzed by nano-CT, histology, and IHC at 2, 4, and 8 weeks. nano-CT analysis of week 2 explants displayed bridging of the defect by a mineralized tissue (Figure 3A). After 4 weeks, the implant had undergone remodeling similar to a cartilaginous callus since a more mineralized structure was seen. After 8 weeks, the fracture was completely bridged and the typically larger intermediate fracture callus was completely remodeled to the original bone's size and mineralized content. Nonunions were confirmed in all controls up to 8 weeks after the creation of the defect (Figure 3B). H&E staining confirmed that the fracture was filled with fibrous, nonmineralized tissue (Figure 3C). Quantification of the reconstructed CT-scans displayed a large callus volume in the week 2 explants, which was reduced with healing time (Figure 3D). In addition, quantification of trabecular number displayed a larger number of trabecular bone spicules in the early callus (Figure 3E). Interestingly, the trabecular thickness increased with fracture healing time (Figure 3F). Qualitative
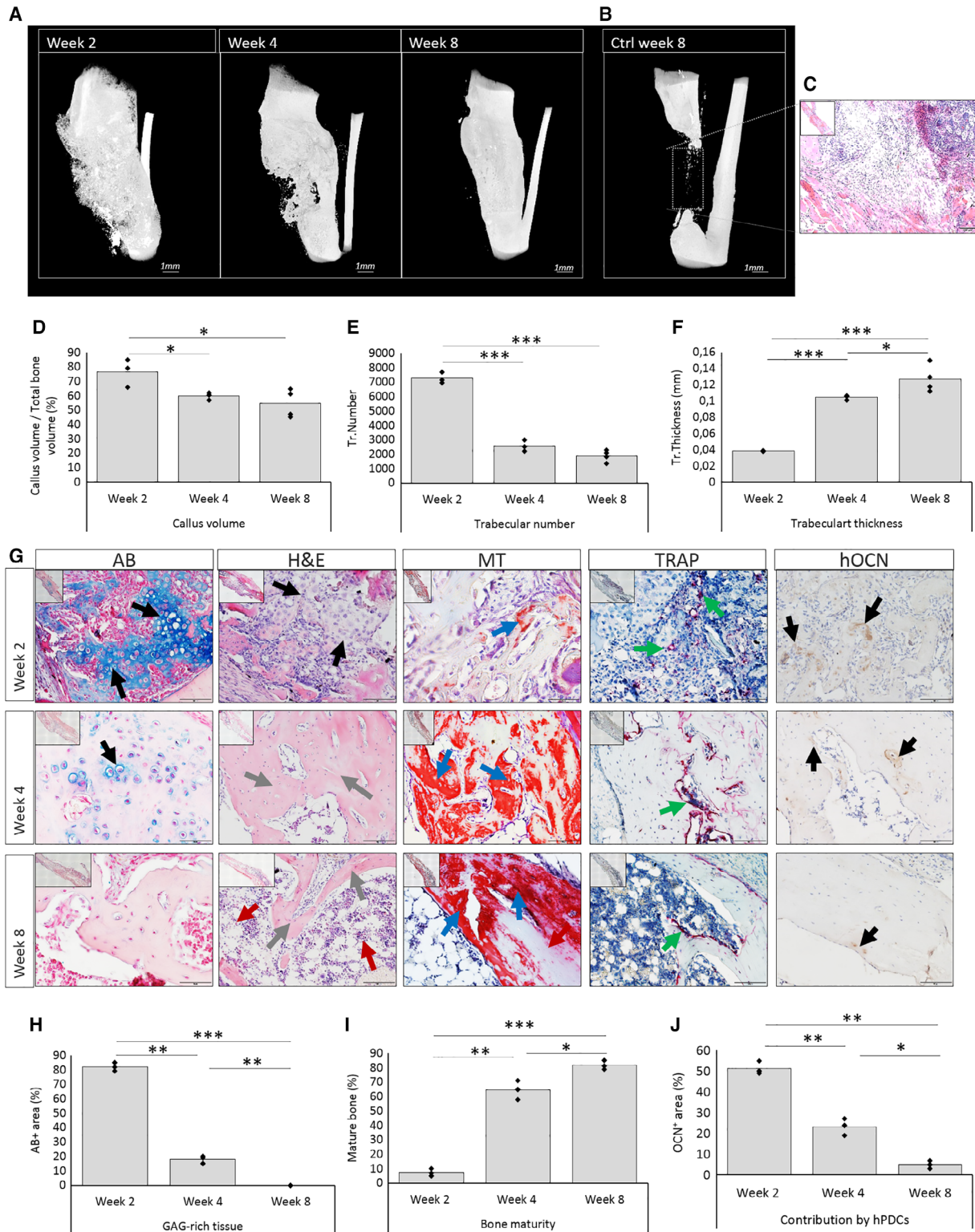
FIGURE 3 Healing of a critical size bone defect by in vitro primed human periosteum-derived cells (hPDCs) when seeded onto a CaP-matrix. hPDCs preconditioned in chemically defined medium (CDM) followed by priming in BMP-2 supplemented CDM and seeded onto a CaP-matrix were implanted in a critical size tibial defect in mice. Fracture healing was investigated at week 2, 4, and 8 by nano-CT (A). The critical size defect was confirmed by implantation of nonstimulated cells on the CaP-matrix (B) where hematoxylin and eosin (H&E) staining confirmed fibrous tissue formation (C). Reconstructed nano-CT images were used to analyze callus volume (D), trabecular number (E), and trabecular thickness (F). Histology confirmed endochondral fracture healing by Alcian blue (AB) staining visualizing GAG-rich areas (black arrows) (G) and quantification (H). H&E staining visualizing *de novo* formed bone (gray arrows), Masson's trichrome (MT) staining confirming bone maturation (blue arrows) (G) and quantification (I). TRAP staining displaying active remodeling (green arrows) and IHC for hOCN confirming contribution of the implanted cells (white arrows) and quantification (J). Statistical significance: *P*-value: * < .05, ** < .01, *** < .001. Scale bar: A-B 1 mm; G: 100 μm
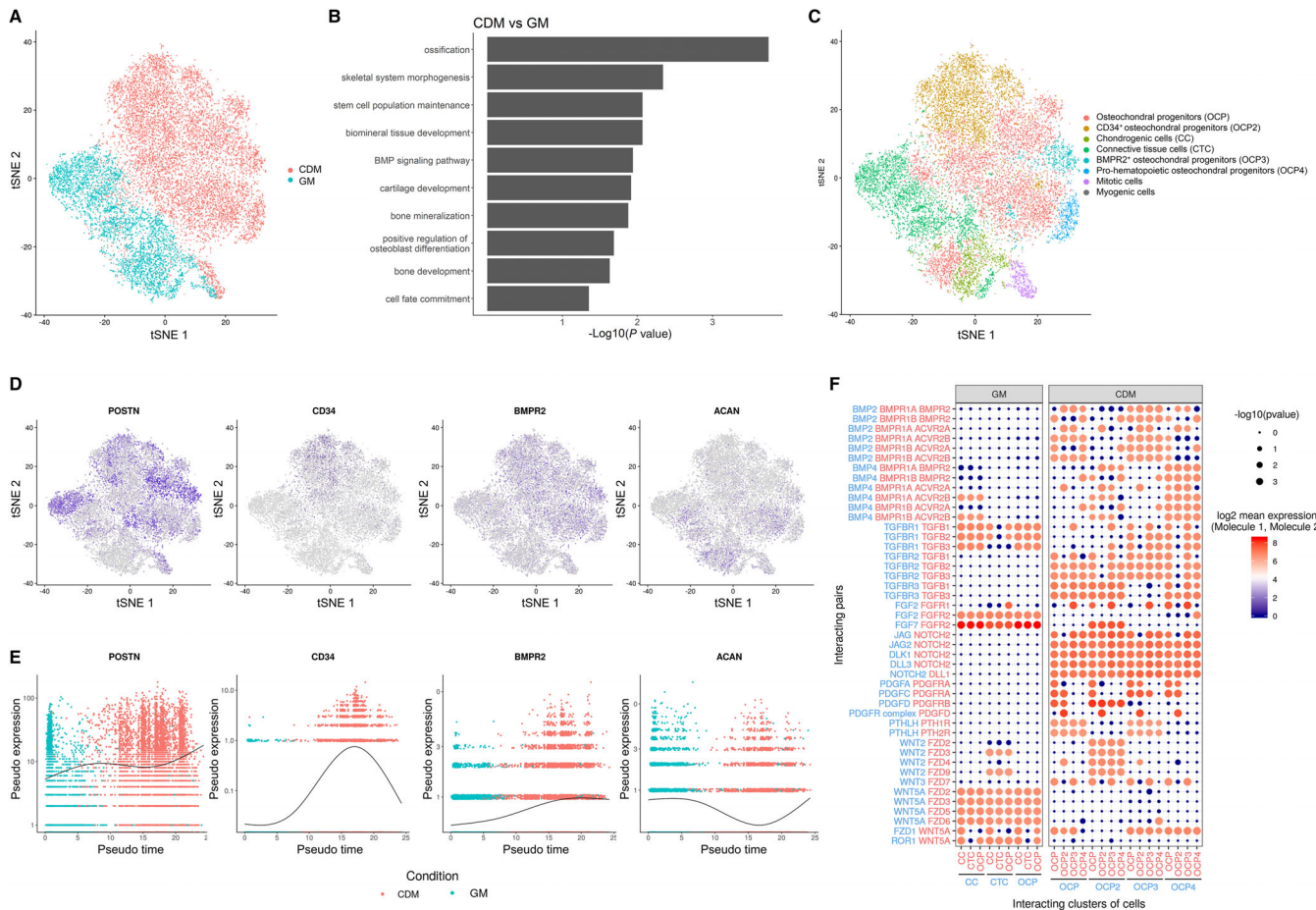
FIGURE 4 Single-cell RNA sequencing reveals a phenotype switch upon chemically defined medium (CDM) preconditioning. Single-cell transcriptomics on human periosteum-derived cells (hPDCs) expanded in growth medium (GM) for 6 days and preconditioned in CDM at day 6 revealed a clear separation of the conditions (A). Genes found differentially expressed between both conditions in a pseudobulk analysis were characterized by gene ontology terms related to osteochondral development (B). Graph-based clustering identified 29 different clusters which were categorized based on their marker expression and marker-associated gene ontology (C). Relative expression of *POSTN*, *CD34*, *BMPR2*, and *ACAN* (D) with corresponding pseudotime expression obtained via unsupervised ordering of hPDCs in GM (blue) and CDM (red) (E). An overview of selected ligand-receptor interactions in the predominant subpopulations of both conditions (F). Circle size reflects *P*-value, and the mean of the average expression of interacting molecules between clusters is indicated by color. CC, chondrogenic cell; CTC, connective tissue cell; OCP, osteochondral progenitor

assessment by Alcian blue staining confirmed the presence of a cartilaginous fracture callus, rich in glycosylated glycosaminoglycans (GAG) at week 2 (black arrows, Figure 3G). At week 4, a reduction in the GAG-rich area was seen and completely vanished by week 8, confirmed by quantification (Figure 3H). H&E staining confirmed that the cartilaginous callus present at week 2 became mineralized and transformed into bone at week 4 (gray arrows), which further matured by week 8, when also bone marrow was present (red arrows). MT staining confirmed the presence of mature mineralized tissues (blue arrows) at all time points. Of note, quantification confirmed that the percentage of mature area increased with fracture healing time (Figure 3I). Remodeling of the cartilaginous matrix was confirmed by TRAP-staining at week 2 (green arrows). Active remodeling was taking place at week 4 and became less pronounced at week 8. Active contribution of the implanted cells was confirmed by IHC for hOCN at week 2 (black arrows) and at week 4, whereas only small positive areas were present in week 8 explants, suggesting that predominantly host cells

contribute to the final remodeling and maturation of the bone tissue (Figure 3J). Combined, these data confirm that in vitro priming of hPDCs in CDM gives rise to more bone formation per cell when seeded onto a CaP-matrix followed by in vivo implantation, and is sufficient to heal a critical size tibial defect in mice.

3.4 | Single-cell RNA sequencing reveals a phenotype switch upon CDM preconditioning

To better understand the underlying mechanism to the elevated bone forming capacity followed by BMP-2 priming at the cellular level, single-cell RNA sequencing (scRNA-seq) was performed in order to obtain a high-resolution map of the hPDC transcriptome in response to CDM preconditioning. Upon visualization in *t*-distributed stochastic neighbor embedding (t-SNE) plots,[19] a clear separation of hPDCs expanded in GM from progenitors preconditioned in CDM could be observed (Figure 4A). When performing a pseudobulk comparison of

both conditions, gene ontology (GO) terms describing the upregulated genes in CDM were associated with skeletal development, stem cell population maintenance, cell fate commitment, and the BMP signaling pathway (Figure 4B). We then performed graph-based clustering and combined cluster-specific markers with their GO terms to annotate the clusters from the CDM and GM population (File S1). This showed that preconditioning in CDM enriches for gene expression profiles associated with specified osteochondrogenic progenitors (Figure 4C and File S1). Gene expression of markers for chondrogenic and osteochondrogenic subpopulations in GM and CDM is shown in Figure 4D. Interestingly, pseudotime analysis obtained via unsupervised ordering of hPDCs in GM (blue) and CDM (red) displayed an increased expression corresponding to the transition from GM to CDM (Figure 4E). Since functional BMP-signaling is indispensable for bone regeneration, we next evaluated the expression of BMP-type 1 receptors and *BMPR2* across all cells and noticed an increased expression profile among preconditioned

osteochondroprogenitor cell (OCP) subpopulations (Figure S5A,B). This was confirmed by Fluorescence-activated cell sorting (FACS; Figure S5C-E). Next, we hypothesized that this phenotype shift could be related to an adaptation of the signaling pathway activity. Therefore, the CellPhoneDB repository[20] was used to predict molecular interactions between cell populations via specific ligand-receptor pairs to generate a potential cell-cell communication network in GM and CDM (Figure 4D). Connective tissue cells, the most abundant cell type in GM, were found to interact predominantly by WNT and fibroblast growth factor. This was abrogated in the OCPs, the most abundant populations in the CDM population. Instead, these cells demonstrated enhanced activity of the BMP, NOTCH and PDGF signaling pathways. Since functional BMP-signaling is indispensable for bone formation and fracture healing, we next evaluated the expression of BMP-receptors in the specific clusters, which demonstrated upregulation in the clusters containing osteochondral progenitors, CD34^{+} progenitors, chondrogenic cells, and BMPR2^{+} osteochondral
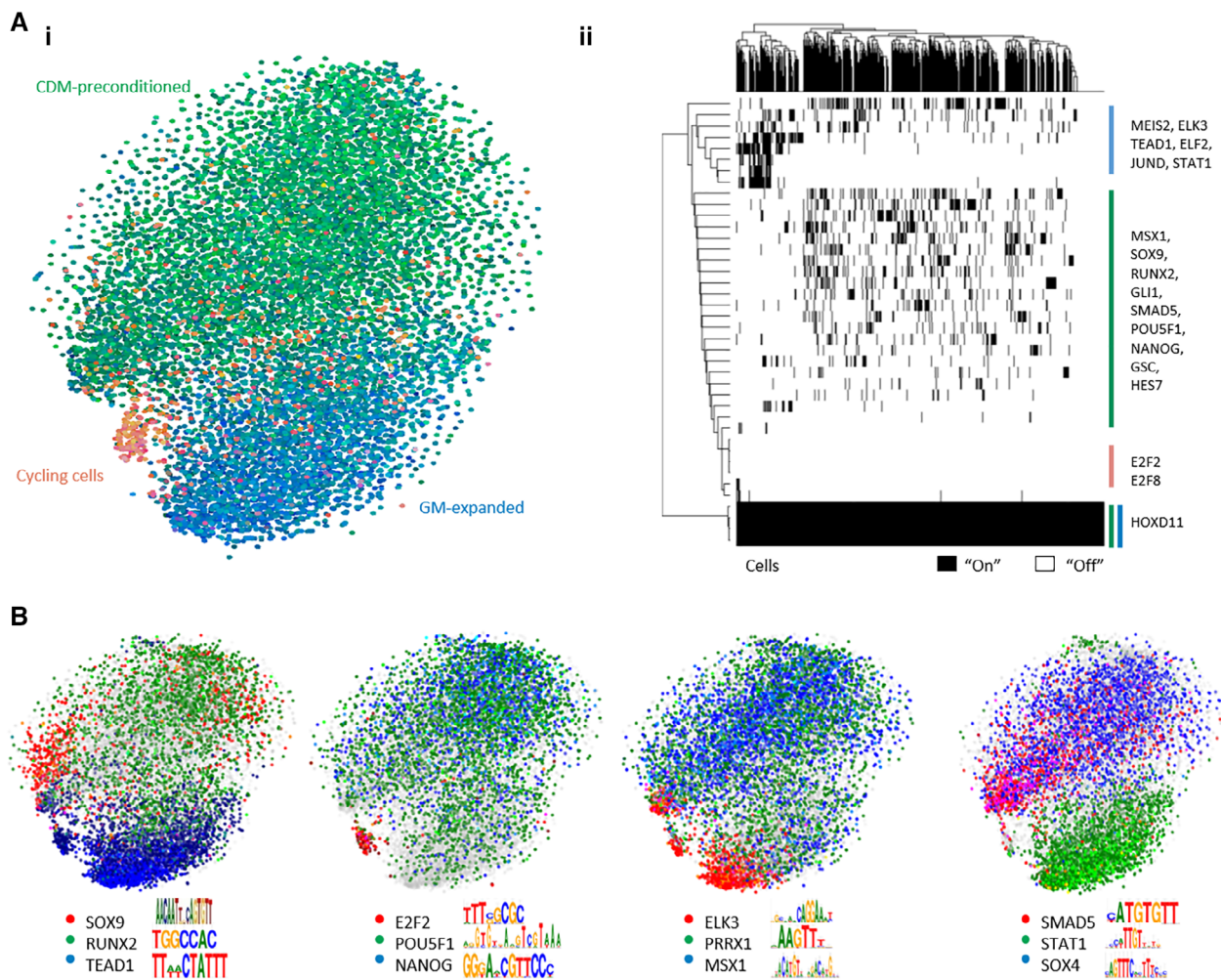

FIGURE 5 Gene regulatory networks related to development and fracture healing underlie the phenotype of preconditioned human periosteum-derived cells (hPDCs). A SCENIC-based t-SNE plot colored by gene regulatory network activity shows three predominant cell states corresponding to the culture conditions and cycling cells (Ai), as defined by the binary regulon activity matrix (Aii). Subpopulations could be identified based on individual regulons: the chemically defined medium (CDM) consists of a SMAD5/SOX9^{high} and a RUNX2/POU5F1/NANOG[high] population (B). The growth medium (GM) was enriched for serum-responsive transcription factors such as TEAD1 and ELK3 as well as the RUNX2 suppressor STAT1

progenitors (Figure 4D). Taken together, the preconditioning in CDM appears to activate physiologically relevant pathways associated with the progenitor cell response to in vivo fracture healing.

3.5 | Genetic signature and transcriptional regulation of the CDM population

The adaptation of gene expression is the result of altered regulatory activity; therefore, we aimed to characterize the TFs involved in the phenotype shift. For this, SCENIC[21] was used to map gene regulatory network activity and cell states. This revealed three robust cell states corresponding to the two culture conditions and cells undergoing mitosis (Figure 5Ai). The state of the GM-cultured cells was driven by TFs including serum-responsive TFs ETS-related transcription factor (ELF)1/2, ETS like-1 protein (ELK3), and transcriptional enhancer factor (TEAD)1; whereas the state of the CDM preconditioned cells was driven by TFs SMAD5, Sex determining region Y-box (SOX)4, SOX9, and Runt-related TF 2 (RUNX2) (Figure 5Aii). The Homeobox-protein (HOXD)11 regulon was predicted to be active in all cells independent of conditions, in correspondence with the tibial origin of the original periosteal biopsies from which the cells were derived. Moreover, a potential gene regulatory network was identified in the CDM population regulated by Msh homeobox (MSX)1, SOX4, and SOX9 (Figure S4A). By analyzing the individual activity of marker TFs, we found two subpopulations in the CDM-preconditioned cells, characterized by either SOX9, SMAD5, or RUNX2 activity. Interestingly, cells with an active RUNX2 regulon appeared to also display enhanced stemness, as seen by the POU5F1 (OCT4) and NANOG regulons (Figure 5B). In contrast, STAT1^{high} cells found in the GM cultured

population were predominantly negative for RUNX2, in accordance with the literature.[22] MSX1 and Paired Related Homeobox (PRRX1), pivotal TFs during limb skeletal development were found in both conditions, but enriched after CDM preconditioning. In addition, regulon activity of SOX4, SOX9, MSX1, and RUNX2 appeared to correlate with gene expression of BMP-receptors *BMPR1A*, *BMPR1B*, and *BMPR2*, the PDGF receptors *PDGFRα*, *PDGFRβ*, and *PDGFRL* as well as ligands from the NOTCH family (Figure S4B-E). This altered regulatory landscape further elucidates the underlying mechanism of the enhanced progenitor cell capacity observed in the CDM population, suggesting the activation of a process that closely mimics the progenitor response seen during in vivo fracture healing.

3.6 | BMPR2^{+} progenitors possess elevated differentiation capacity

Next, we aimed to define a biologically relevant marker for the potent progenitor population generated by the CDM preconditioning. BMP-signaling was one of the processes that was frequently upregulated in the CDM-clusters as seen by the GO analysis. Since BMP-ligands are crucial during fracture healing and signal through a receptor complex, we evaluated the expression of BMP receptors by flow cytometry in the CDM and GM populations (Figure S5). BMPR2 displayed a significantly higher expression in CDM cultures in terms of expressing cells, as well as number of receptors per cell. In order to elucidate the potency of the BMPR2^{+} hPDC population, FACS was used to enrich for a BMPR2^{+} population after 6 days of CDM preconditioning (Figure 6A). The purity of the BMPR2^{+} and BMPR2^{−} populations was confirmed by flow cytometry (Figure 6B). Next, the sorted BMPR2^{+}
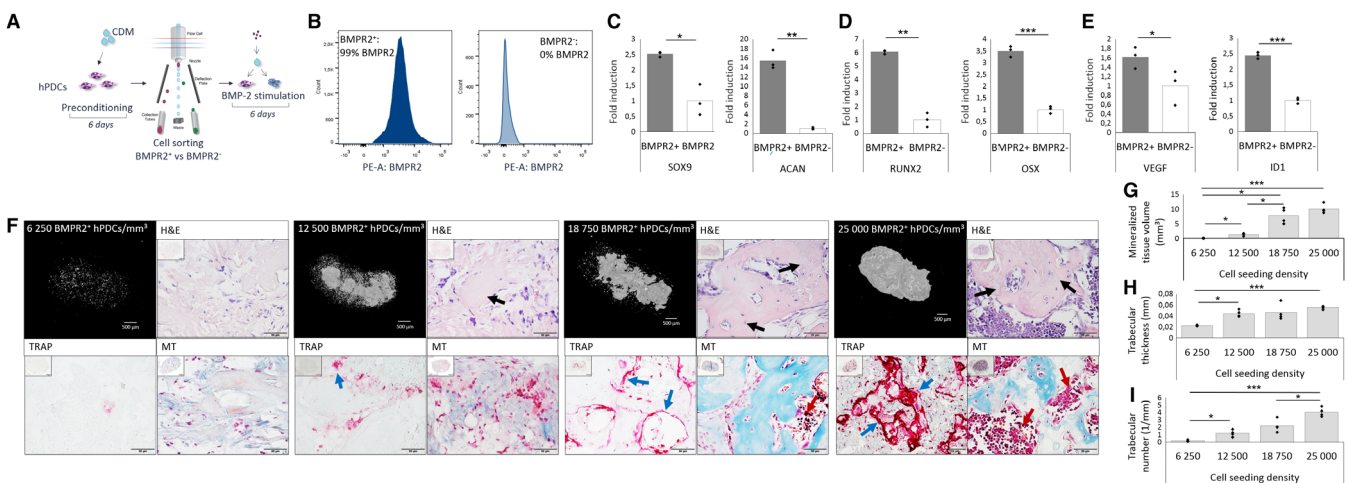

FIGURE 6 Enhanced differentiation and bone forming potential in BMPR2^{+}-progenitors. BMPR2^{+} human periosteum-derived cells (hPDCs) preconditioned in chemically defined medium (CDM) were sorted by flow cytometry (A) and purity was confirmed in BMPR2^{+} and BMPR2^{−} populations (B). Sorted cells were seeded for stimulation in BMP-2 supplemented CDM followed by mRNA transcript analysis for chondrogenic (*SOX9* and *ACAN*) (C) and osteogenic (*RUNX2* and *OSX*) lineage markers (D) and marker for vascular recruitment (*VEGF*) and BMP-target gene *ID1* (E). *In vitro* primed BMPR2^{+} hPDCs were then seeded onto a CaP-matrix at 25, 18.75, 12.5, and 6.25×10^3 cells/mm^{3} scaffold followed by subcutaneous implantation. Reconstructed nano-CT images display three-dimensional (3D) images of *de novo* mineralized tissue and qualitative analysis by hematoxylin and eosin (H&E), Masson's trichrome (MT) and TRAP of explants for bone (black arrows), bone marrow (red arrows), and remodeling (blue arrows) harvested 4 weeks after implantation (F). Quantification of mineralized tissue volume (G), trabecular thickness (H), and trabecular number (I). Statistical significance: *P*-value: * < .05, ** < .01, *** < .001. Scale bar: reconstructed 3D CT images: 500 μm, histology: 50 μm

and BMPR2⁻ populations were cultured separately for another 6 days in BMP-2 supplemented CDM and osteochondrogenic differentiation was investigated by mRNA transcript analysis. Elevated mRNA transcript levels of the chondrogenic markers *SOX9* and *ACAN* was seen in the BMPR2⁺ enriched population when compared with the BMPR2⁻ population (Figure 6C). In parallel, elevated expression in the BMPR2⁺ population was also seen for the osteogenic markers *RUNX2*

and *OSX* (Figure 6D), as well as for the vascular recruiter *VEGF* and BMP target gene *ID1* (Figure 6E).

In order to investigate whether the BMPR2⁺ enriched cell population possessed elevated in vivo bone forming capacity compared with unsorted cells, BMP-2 stimulated BMPR2⁺-cells were seeded onto a CaP-matrix at densities for which we had previously established that unsorted cells were incapable of forming bone (Figure 2H). These
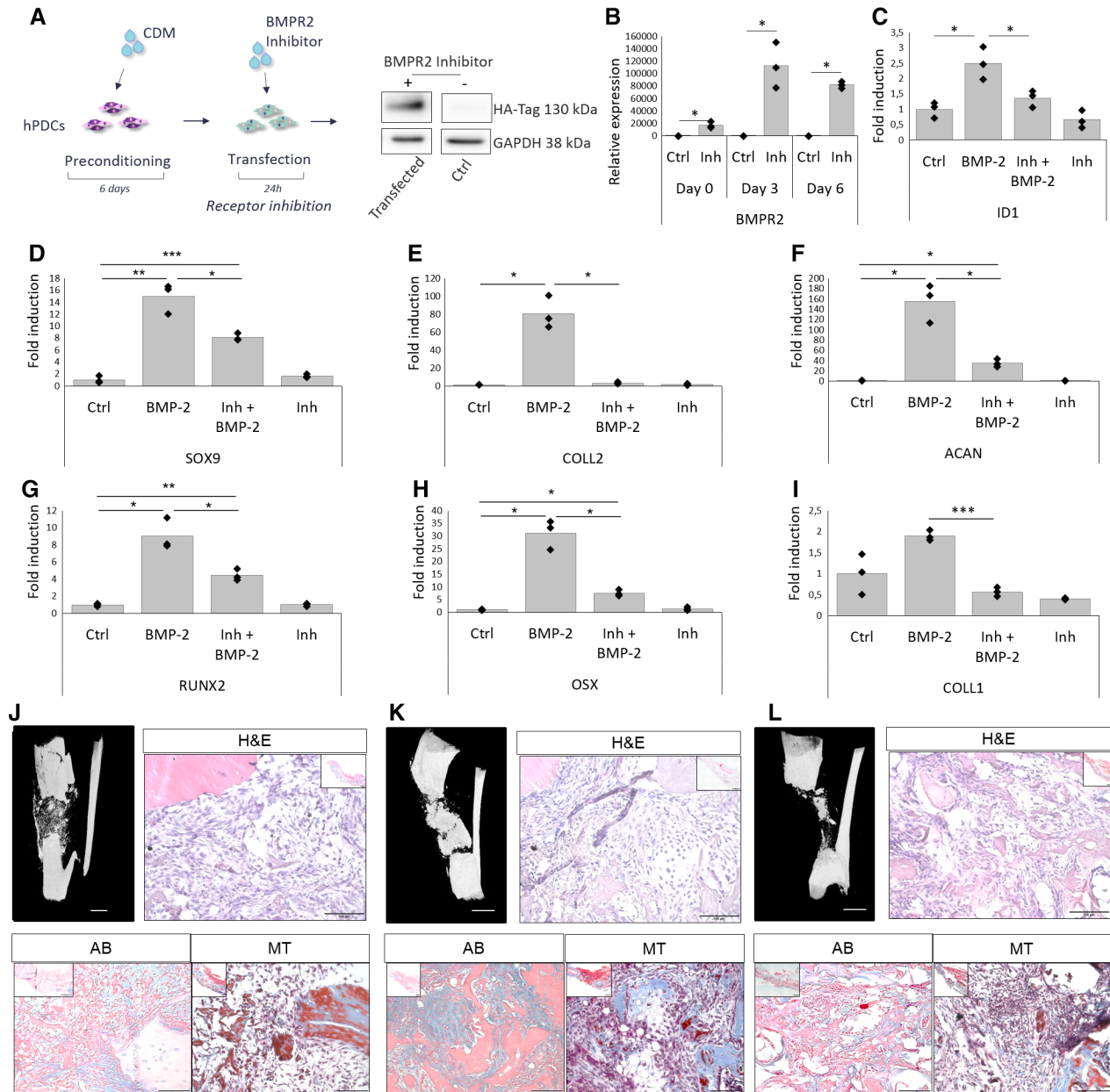

FIGURE 7 Functional BMPR2-signaling is required for hPDC-mediated fracture healing. Human periosteum-derived cells (hPDCs) preconditioned in chemically defined medium (CDM) was transfected with a HA-tagged overexpressing BMPR2 mutant functioning as an inhibitor (Inh) followed by BMP-2 stimulation. Functional transfection was confirmed by Western blot (A) and overexpression of BMPR2 was confirmed by mRNA transcript analysis up to 6 days (B). Analysis of impaired in vitro differentiation in the transfected cells (Inh and Inh + BMP-2) was associated with decreased mRNA transcripts for *ID1* (C) and chondrogenic markers *SOX9* (D), *COLL2* (E), *ACAN* (F), and osteogenic markers *RUNX2* (G), *OSX* (H), and *COLL1* (I). Implantation of the transfected cells followed by BMP-2 stimulation and seeding onto a CaP-matrix in a critical size tibial defect in mice impaired fracture healing, as visualized by nano-CT and histology for hematoxylin and eosin (H&E), Alcian blue (AB), and Masson's trichrome (MT) at week 2 (J), week 4 (K), and week 8 (L). Statistical significance: *P*-value: * < .05, ** < .01, *** < .001. Scale bar: reconstructed three-dimensional CT images: 1 mm, histology: 100 μm

constructs, loaded with 25,000, 18,750, 12,500, and 6,250 primed BMPR2+ hPDCs/mm^3, were then ectopically implanted in a nude mouse model. Bone formation was investigated 4 weeks after implantation by nano-CT and histology. Reconstructed nano-CT scans displayed homogeneous and robust formation of *de novo* mineralized tissue at 25,000 and 18,750 hPDCs/mm^3 scaffold, whereas homogeneous but less evenly distributed bone was observed in 12,500 hPDCs/mm^3 scaffold and only limited mineralization was found in 6250 hPDCs/mm^3 scaffold (Figure 6F). Subsequently, *de novo*-formed bone was confirmed by histological analysis for H&E, MT, and TRAP. Quantification of the reconstructed nano-CT images displayed increased *de novo*-mineralized tissue formation with increasing cell seeding density (Figure 6G). Moreover, no difference between trabecular thickness could be seen between the three bone forming conditions (Figure 6H). However, trabecular number displayed elevated numbers with increasing cell seeding (Figure 6I). Upon histological evaluation, robust bone formation was confirmed in conditions containing 25,000 and 18,750, limited in 12,500 while none in 6250 hPDCs/mm^3 CaP matrix (Figure 6J). Combined, these data suggest that BMPR2 represents a relevant marker to be used for the enrichment of a potent bone-forming population of *in vitro*-expanded periosteum derived progenitor cells.

3.7 | Functional BMPR2 expression is crucial for hPDC-mediated fracture healing

The importance of the upregulated functional expression of BMPR2 in CDM cultures was investigated by transfecting CDM preconditioned hPDCs with a BMPR2 mutant, functioning as a silencer when overexpressed. Functional transfection was confirmed by Western blot for the HA-tagged BMPR2 mutant on protein level (Figure 7A). In addition, mutant BMPR2 overexpression was confirmed in the transfected cells (Inh) on mRNA transcript level 16 hours after transfection. This overexpression was stable for at least 6 days, which represents the time of preconditioning (Figure 7B). Expression of *ID1*, a target gene of the BMP signaling pathway, confirmed the loss of BMP responsiveness in transfected hPDCs (Figure 7C). Thereafter, transfected cells were stimulated in BMP-2 supplemented CDM for 6 days. A twofold downregulation of the chondrogenic marker *SOX9* was seen in the transfected cells (Figure 7D). Analysis of the cartilaginous matrix marker *COLL2* displayed an over 10-fold downregulation (Figure 7E). In addition, *ACAN* displayed a fourfold decrease in the cultures transfected with the BMPR2 mutant (Figure 7F). Analysis of *RUNX2* and *OSX* also displayed an inhibition in the transfected cells upon BMP-2 stimulation (Figure 7G,H). Moreover, the osteogenic matrix marker *COLL1* displayed an over fourfold downregulation in the transfected cells upon BMP-2 stimulation (Figure 7I). By seeding the transfected, BMP-2–stimulated cells onto a CaP matrix followed by implantation into a critical size tibial defect in nude mice, the fracture healing potential was investigated. Analysis 2 weeks after implantation displayed no formation of a mineralized callus (Figure 7J). At 4 weeks, some mineralized zones could be seen, without any connection between the formed spicules (Figure 7K). At week 8, impaired fracture healing was confirmed since no bridging of the two bone ends could

be observed (Figure 7L). Combined, these data suggest that functional BMPR2-signaling is crucial for the osteochondrogenic and bone forming capacity in CDM preconditioned hPDCs.

4 | DISCUSSION

The success of cell-based constructs developed for regenerative medicine has been hampered largely due to a nonreliable in vivo biological potency of the implant.[23] This has been associated with a lack of in depth characterization of the in vitro product and its relation to in vivo potency. In terms of cell-based constructs, the cells provide the driving force for the construct's tissue forming capacity by direct or paracrine contributions to the newly formed tissue.[3] Consequently, nonreliable behavior of the construct has been associated with a lack of control over progenitor cell commitment during the in vitro preimplantation stage, due to nonoptimal culture conditions.[15,24,25] Herein, we characterized the mechanism on a cellular, molecular, and transcriptional basis of an improved differentiation capacity generated by serum-free preconditioning of *in vitro*-expanded hPDCs. Captivatingly, we also explored at the single-cell level how the preconditioned cells underwent a phenotype switch toward more potent skeletal progenitor cells.

Upon seeding the serum-free preconditioned and in vitro BMP-2 primed cells onto a CaP-matrix followed by in vivo implantation, a significantly higher bone forming capacity was seen as compared with GM conditions. In addition, the bone forming process was shown to follow the endochondral pathway, in line with a bioinspired healing strategy for the treatment of long bone fractures.[4] This was further confirmed since implantation into a critical size long bone defect in mice displayed fracture healing through the formation of an intermediate cartilaginous callus with successful bridging within 4 weeks after implantation. This potent effect of a short in vitro priming period displays how powerful the right combination of progenitor cells and preconditioning followed by stimulation can be. This is of notable interest for pleiotropic growth factors such as BMP ligands, for which the safety has been debated in recent years due to the implantation of supraphysiological doses.[26] The potency of solely in vitro priming on the other hand has shown limited success due to insufficient tissue formation *in vivo*,[27] likely due to a heterogeneous and noncommitted progenitor population.[28] In attempts to overcome this, prolonged differentiation time increases the maturity thus potentially also in vivo tissue formation, but challenges integration at the defect site upon implantation.[28,29] The herein presented in vitro priming of progenitor cells generates a clear enrichment in specified skeletal progenitors. This leads to secretion of crucial signaling molecules that upon implantation can function in a paracrine signaling manner with both graft- and host-derived progenitors, allowing for full integration and further remodeling at the fracture site.[12]

Recruitment of osteochondrogenic precursor cells to the fracture site relies on a strictly controlled temporal and spatial chemotactic navigation of signals. In this setting, secreted growth and differentiation factors play a crucial role.[12,30–34] Commonly, these soluble factors signal through cell

surface receptors. Subsequently, the stimulatory effect of the growth factor ligand is directly correlated to the presence and availability of the specific receptors on the cell surface.[35] Once signaling is activated, the combined effect of the growth factors affects progenitor cell migration, proliferation, lineage determination, differentiation, survival, and/or activity. Therefore, it can be speculated that expressed signaling pathway receptors, not yet occupied by cell-secreted growth factors, may be interesting markers for the enrichment of a more specified progenitor cell population.[36] Through a detailed characterization, we could define BMPR2 as a cell surface marker associated with the increased osteochondrogenic potential seen in the CDM preconditioned cells, but not yet fully used by growth factors secreted by the cells. The elevated capacity induced by BMP-2 stimulation was further supported by an increased expression of VE-cadherin, a molecule shown to stabilize the BMP-receptor-ligand complex.[37] In addition, in vivo implantation of BMPR2^{+} sorted hPDCs confirmed the increased cell differentiation potential. This was shown by maintained bone forming capacity with reduced cell seeding density, since sufficient cell numbers have been proven crucial for a construct's bone forming capacity.[38] In line with previous findings, a further reduction in cell numbers imperiled reliable bone formation.[39] Furthermore, when BMPR2 was silenced through dominant negative BMPR2 (dnBMPR2) expression, compromised in vitro differentiation and in vivo bone formation were seen. Downstream BMPR2 signaling is determined at the cell membrane level subjected to the formation of heterodimer/homodimer complex formation with the type 1 receptor, and the complex inducing or subsequent binding of the BMP-2 ligand.[40,41] It is not clear at what level the dnBMPR2 affected this complex formation in the investigated cells. However, due to the significantly reduced differentiation capacity seen in the investigated cells, it is anticipated that the downstream signaling from potential homo- as well as heterodimers was affected. Of note, the crucial importance of BMPR2 in periosteal cells is in line with previous research where BMPR2 was shown to be expressed by cells associated with fracture healing.[42] Of particular interest, BMPR2 was specifically strongly expressed by cells located within the thickening of the periosteum adjacent to the fracture 3 days after fracture.

During fracture repair, resting progenitor cells from the periosteum are recruited to the fracture site to undergo massive proliferation and differentiation upon the accurate signaling instructions.[42,43] In this setting, their energy and redox metabolism is adapted in order to survive in hypoxic and nutrient deprived conditions.[43] These adaptations were previously characterized in mouse PDCs.[44] Interestingly, hypoxic culture conditions were shown to provoke recruitment of the glycogen stores to maintain the energy balance. Concomitantly, redox homeostasis was preserved by increased uptake of glutamine, which was subsequently converted into glutamate by *GLS1* for glutathione biosynthesis. These combined adjustments resulted in increased cell survival and bone forming capacity in vivo. Preconditioning in CDM followed by stimulation with BMP-2 seems to induce a similar metabolic adaptation, as gene expression of the glycogen recruiting protein *PYGL* was significantly increased. Moreover, addition of BMP-2 appeared to impose an increased demand for reductive potential, reflected by the elevated transcription of *PRPS1* and *GLS1*.

To confirm whether the enhanced cell potency was due to cellular reprogramming at the single cell level, single-cell RNA sequencing was performed. Interestingly, preconditioning in CDM was demonstrated to induce a clear phenotype switch with elevated expression of markers and signaling clusters associated with skeletal system development, tissue regeneration, stem cell maintenance, cell fate commitment, and the BMP-signaling pathway. Upon clustering of the complete data set, it was shown that the individual clusters from CDM origin displayed elevated markers and processes related to osteochondral progenitor cells. On the other hand, the majority of the GM-originated clusters displayed markers and elevated processes related to connective tissue, once again confirming the more homogenous and osteochondro-specific progenitor commitment in the CDM population. Detailed analysis on the transcriptional level confirmed upregulated and active involvement of the regulon SOX4, SOX9, MSX1, and RUNX2 regulons to the enhanced potential in the CDM population. These data are in line with recent findings mapping the hierarchy of human skeletal stem and progenitor cells present in the human foetus, but also activated during postnatal fracture repair.[45] However, the preconditioned progenitors described and characterized herein are most likely further committed in their osteochondrogenic specification, since the majority of the cells do not proliferate in the absence of BMP-2.

In conclusion, our findings suggest that the CDM preconditioning of hPDCs induced a phenotype switch of the in vitro serum expanded progenitor cells, leading to a more potent bone forming cell population when assessed in vivo. Interestingly, cell characterization was associated with an elevated expression of markers related to limb development and fracture healing. Specifically, the presence and activity of BMPR2 appears crucial for the improved in vivo bone forming capacity of the cells. In addition, the improved cell differentiation was associated with a cellular switch toward a more efficient metabolism, potentially related to the elevated resistance to harsh conditions as encountered during in vivo implantation. These findings support the importance of the appropriate design and development of cell-based constructs. Moreover, the presented data reflect how crucial the in vitro culture conditions are for the in vivo outcome and hence open up new opportunities and perspectives for the characterization and regulation of cell-based products.

the Hercules Foundation (project AKUL 09/001: Micro-and nano-CT for the hierarchical analysis of materials).

CONFLICT OF INTEREST

AUTHOR CONTRIBUTIONS

J.B.: conception and design, financial support, administrative support, collection and assembly of data, manuscript writing, data analysis and interpretation, and final approval of manuscript; T.H.: collection and assembly of data, manuscript writing, and final approval of manuscript; M.C.: final approval of manuscript, collection of data, and data analysis; C.G.: final approval of manuscript and assembly of data; L.G.: final approval of manuscript and data interpretation; F.P.L.: conception and design, financial support, data analysis and interpretation, and final approval of manuscript.

DATA AVAILABILITY STATEMENT

The scRNA-seq files reported in this paper are available at the Gene Expression Omnibus (GEO), project accession number GSE138791.

ORCID

Johanna Bolander https://orcid.org/0000-0002-6915-9509

REFERENCES

1. Langer R, Vacanti J. Tissue engineering. *Science*. 1993;260:920-926.
2. Ma J, Both SK, Yang F, et al. Concise review: cell-based strategies in bone tissue engineering and regenerative medicine. STEM CELLS TRANSLATIONAL MEDICINE. 2014;3:98-107. https://doi.org/10.5966/sctm.2013-0126.
3. Ho-Shui-Ling A, Bolander J, Rustom LE, Johnson AW, Luyten FP, Picart C. Bone regeneration strategies: engineered scaffolds, bioactive molecules and stem cells current stage and future perspectives. *Biomaterials*. 2018;180:143-162. https://doi.org/10.1016/j.biomaterials.2018.07.017.
4. Lenas P, Moos M, Luyten FP. Developmental engineering: a new paradigm for the design and manufacturing of cell-based products. Part I: from three-dimensional cell growth to biomimetics of in vivo development. *Tissue Eng Part B Rev*. 2009;15:381-394. https://doi.org/10.1089/ten.TEB.2008.0575.
5. Ingber DE, Mow VC, Butler D, et al. Tissue engineering and developmental biology: going biomimetic. *Tissue Eng*. 2006;12:3265-3283. https://doi.org/10.1089/ten.2006.12.3265.
6. Einhorn TA, Gerstenfeld LC. Fracture healing: mechanisms and interventions. *Nat Rev Rheumatol*. 2015;11:45-54. https://doi.org/10.1038/nrrheum.2014.164.
7. Colnot C. Skeletal cell fate decisions within periosteum and bone marrow during bone regeneration. *J Bone Miner Res*. 2009;24:274-282. https://doi.org/10.1359/jbmr.081003.
8. Colnot C, Zhang X, Knothe Tate ML. Current insights on the regenerative potential of the periosteum: molecular, cellular, and endogenous engineering approaches. *J Orthop Res*. 2012;30:1869-1878. https://doi.org/10.1002/jor.22181.
9. Chappuis V, Gamer L, Cox K, Lowery JW, Bosshardt DD, Rosen V. Periosteal BMP2 activity drives bone graft healing. *Bone*. 2012;51:800-809. https://doi.org/10.1016/j.bone.2012.07.017.
10. Bolander J, Chai YC, Geris L, et al. Early BMP, Wnt and Ca(2+)/PKC pathway activation predicts the bone forming capacity of periosteal cells in combination with calcium phosphates. *Biomaterials*. 2016;86:106-118. https://doi.org/10.1016/j.biomaterials.2016.01.059.
11. Bolander J, Ji W, Geris L, et al. The combined mechanism of bone morphogenetic protein- and calcium phosphate-induced skeletal tissue formation by human periosteum derived cells. *Eur Cells Mater*. 2016;31:11-25.
12. Bolander J, Ji W, Leijten J, et al. Healing of a large long-bone defect through serum-free Iin vitro priming of human periosteum-derived cells. *Stem Cell Rep*. 2017;8:758-772. https://doi.org/10.1016/j.stemcr.2017.01.005.
13. Salazar VS, Capelo LP, Cantù C, et al. Reactivation of a developmental Bmp2 signaling center is required for therapeutic control of the murine periosteal niche. *Elife*. 2019;8:e42386. https://doi.org/10.7554/eLife.42386.
14. Salazar VS, Gamer LW, Rosen V. BMP signalling in skeletal development, disease and repair. *Nat Rev Endocrinol*. 2016;12:203-221. https://doi.org/10.1038/nrendo.2016.12.
15. International Stem Cell Initiative Consortium, Akopian V, Andrews PW, et al. Comparison of defined culture systems for feeder cell free propagation of human embryonic stem cells. *In Vitro Cell Dev Biol Anim*. 2010;46:247-258. https://doi.org/10.1007/s11626-010-9297-z.
16. Verbeeck L, Geris L, Tylzanowski P, Luyten FP. Uncoupling of in-vitro identity of embryonic limb derived skeletal progenitors and their in-vivo bone forming potential. *Sci Rep*. 2019;9:5782. https://doi.org/10.1038/s41598-019-42259-x.
17. Yang PJ, Yuan WX, Liu J, et al. Biological characterization of human amniotic epithelial cells in a serum-free system and their safety evaluation. *Acta Pharmacol Sin*. 2018;39:1305-1316. https://doi.org/10.1038/aps.2018.22.
18. Trapnell C, Cacchiarelli D, Grimsby J, et al. The dynamics and regulators of cell fate decisions are revealed by pseudotemporal ordering of single cells. *Nat Biotechnol*. 2014;32:381-386. https://doi.org/10.1038/nbt.2859.
19. Platzer A. Visualization of SNPs with t-SNE. *PLoS One*. 2013;8:e56883. https://doi.org/10.1371/journal.pone.0056883.
20. Vento-Tormo R, et al. Single-cell reconstruction of the early maternal-fetal interface in humans. *Nature*. 2018;563:347-353. https://doi.org/10.1038/s41586-018-0698-6.
21. Aibar S, et al. SCENIC: single-cell regulatory network inference and clustering. *Nat Methods*. 2017;14:1083-1086. https://doi.org/10.1038/nmeth.4463.
22. Kim S, et al. Stat1 functions as a cytoplasmic attenuator of Runx2 in the transcriptional program of osteoblast differentiation. *Genes Dev*. 2003;17:1979-1991. https://doi.org/10.1101/gad.1119303.
23. Featherall J, Robey PG, Rowe DW. Continuing challenges in advancing preclinical science in skeletal cell-based therapies and tissue regeneration. *J Bone Miner Res*. 2018;33:1721-1728. https://doi.org/10.1002/jbmr.3578.
24. Berger MG, et al. Cell culture medium composition and translational adult bone marrow-derived stem cell research. STEM CELLS. 2006;24:2888-2890. https://doi.org/10.1634/stemcells.2006-0387.
25. Dimarakis I, Levicar N. Cell culture medium composition and translational adult bone marrow-derived stem cell research. STEM CELLS. 2006;24:1407-1408. https://doi.org/10.1634/stemcells.2005-0577.
26. Lowery JW, Rosen V. Bone morphogenetic protein-based therapeutic approaches. *Cold Spring Harb Perspect Biol*. 2018;10:a022327. https://doi.org/10.1101/cshperspect.a022327.
27. Knuth CA, Witte-Bouma J, Ridwan Y, Wolvius EB, Farrell E. Mesenchymal stem cell-mediated endochondral ossification utilising micropellets and brief chondrogenic priming. *Eur Cell Mater*. 2017;34:142-161. https://doi.org/10.22203/eCM.v034a10.
28. Eyckmans J, et al. Mapping calcium phosphate activated gene networks as a strategy for targeted osteoinduction of human

progenitors. *Biomaterials*. 2013;34:4612-4621. https://doi.org/10.1016/j.biomaterials.2013.03.011.

29. Yamashita A, et al. Generation of scaffoldless hyaline cartilaginous tissue from human iPSCs. *Stem Cell Rep*. 2015;4:404-418. https://doi.org/10.1016/j.stemcr.2015.01.016.

30. Colciago A, et al. In vitro effects of PDGF isoforms (AA, BB, AB and CC) on migration and proliferation of SaOS-2 osteoblasts and on migration of human osteoblasts. *Int J Biomed Sci*. 2009;5:380-389.

31. Fiedler J, Etzel N, Brenner RE. To go or not to go: migration of human mesenchymal progenitor cells stimulated by isoforms of PDGF. *J Cell Biochem*. 2004;93:990-998. https://doi.org/10.1002/jcb.20219.

32. Godwin SL, Soltoff SP. Extracellular calcium and platelet-derived growth factor promote receptor-mediated chemotaxis in osteoblasts through different signaling pathways. *J Biol Chem*. 1997;272:11307-11312.

33. Canalis E, Varghese S, McCarthy TL, Centrella M. Role of platelet derived growth factor in bone cell function. *Growth Regul*. 1992;2:151-155.

34. Li G, Cui Y, McIlmurray L, Allen WE, Wang H. rhBMP-2, rhVEGF(165), rhPTN and thrombin-related peptide, TP508 induce chemotaxis of human osteoblasts and microvascular endothelial cells. *J Orthop Res*. 2005;23:680-685. https://doi.org/10.1016/j.orthres.2004.12.005.

35. Yadin D, Knaus P, Mueller TD. Structural insights into BMP receptors: specificity, activation and inhibition. *Cytokine Growth Factor Rev*. 2016;27:13-34. https://doi.org/10.1016/j.cytogfr.2015.11.005.

36. Deveza L, Ortinau L, Lei K, Park D. Comparative analysis of gene expression identifies distinct molecular signatures of bone marrow- and periosteal-skeletal stem/progenitor cells. *PLoS One*. 2018;13:e0190909. https://doi.org/10.1371/journal.pone.0190909.

37. Benn A, Bredow C, Casanova I, Vukicevic S, Knaus P. VE-cadherin facilitates BMP-induced endothelial cell permeability and signaling. *J Cell Sci*. 2016;129:206-218. https://doi.org/10.1242/jcs.179960.

38. Eyckmans J, Roberts SJ, Schrooten J, Luyten FP. A clinically relevant model of osteoinduction: a process requiring calcium phosphate and BMP/Wnt signalling. *J Cell Mol Med*. 2010;14:1845-1856. https://doi.org/10.1111/j.1582-4934.2009.00807.x.

39. Mao AS, Shin JW, Mooney DJ. Effects of substrate stiffness and cell-cell contact on mesenchymal stem cell differentiation. *Biomaterials*. 2016;98:184-191. https://doi.org/10.1016/j.biomaterials.2016.05.004.

40. Nohe A, et al. The mode of bone morphogenetic protein (BMP) receptor oligomerization determines different BMP-2 signaling pathways. *J Biol Chem*. 2002;277:5330-5338. https://doi.org/10.1074/jbc.M102750200.

41. Dorpholz G, et al. IRS4, a novel modulator of BMP/Smad and Akt signalling during early muscle differentiation. *Sci Rep*. 2017;7:8778. https://doi.org/10.1038/s41598-017-08676-6.

42. Onishi T, Ishidou Y, Nagamine T, et al. Distinct and overlapping patterns of localization of bone morphogenetic protein (BMP) family members and a BMP type II receptor during fracture healing in rats. *Bone*. 1998;22:605-612.

43. Riddle RC, Clemens TL. Bone cell bioenergetics and skeletal energy homeostasis. *Physiol Rev*. 2017;97:667-698. https://doi.org/10.1152/physrev.00022.2016.

44. Stegen S, et al. HIF-1alpha promotes glutamine-mediated redox homeostasis and glycogen-dependent bioenergetics to support postimplantation bone cell survival. *Cell Metab*. 2016;23:265-279. https://doi.org/10.1016/j.cmet.2016.01.002.

45. Chan CKF, et al. Identification of the human skeletal stem cell. *Cell*. 2018;175:43-56.e21. https://doi.org/10.1016/j.cell.2018.07.029.

SUPPORTING INFORMATION

Additional supporting information may be found online in the Supporting Information section.

How to cite this article: Bolander J, Herpelinck T, Chaklader M, Gklava C, Geris L, Luyten FP. Single-cell characterization and metabolic profiling of in vitro cultured human skeletal progenitors with enhanced in vivo bone forming capacity. *STEM CELLS Transl Med*. 2020;9:389–402. https://doi.org/10.1002/sctm.19-0151